

Quantum imaginary-time control for accelerating the ground-state preparation

Yu-Cheng Chen,^{1,2} Yu-Qin Chen,^{1,*} Alice Hu,^{2,3,†} Chang-Yu Hsieh,^{1,4,‡} and Shengyu Zhang¹

¹Tencent Quantum Laboratory, Tencent, Shenzhen, Guangdong 518057, China

²Department of Mechanical Engineering, City University of Hong Kong, Hong Kong SAR 999077, China

³Department of Materials Science and Engineering, City University of Hong Kong, Kowloon, Hong Kong SAR 999077, China

⁴Innovation Institute for Artificial Intelligence in Medicine of Zhejiang University, College of Pharmaceutical Sciences, Zhejiang University, Hangzhou 310058, China



(Received 27 December 2021; revised 10 March 2023; accepted 21 March 2023; published 10 May 2023)

Quantum computers have been widely speculated to offer significant advantages in obtaining the ground state of difficult Hamiltonian in chemistry and physics. In this work, we first propose a Lyapunov control-inspired strategy to accelerate the well-established imaginary-time method for ground-state preparation. We also dig for the source of acceleration of the imaginary-time process under Lyapunov control with theoretical understanding and dynamic process visualization. To make the method accessible in the noisy intermediate-scale quantum era, we further propose a variational form of the algorithm that could work with shallow quantum circuits. Through numerical experiments on a broad spectrum of realistic models, including molecular systems, 2D Heisenberg models, and Sherrington-Kirkpatrick models, we show that imaginary-time control may substantially accelerate the imaginary-time evolution for all systems and even generate orders of magnitude acceleration (suggesting order-of-magnitude acceleration) for challenging molecular Hamiltonians involving small energy gaps as impressive special cases. Finally, with a proper selection of the control Hamiltonian, the new variational quantum algorithm does not incur additional measurement costs compared to the original variational quantum imaginary-time algorithm.

DOI: [10.1103/PhysRevResearch.5.023087](https://doi.org/10.1103/PhysRevResearch.5.023087)

I. INTRODUCTION

Quantum computing holds great promise to accelerate essential computational tasks in many fields, such as cryptography, finance, chemistry, material science, and machine learning [1–4]. Particularly, using a quantum computer to solve chemical problems is deemed one of the most promising areas to first witness a practical quantum advantage [4] against classical algorithms. For instance, many efforts have been invested in devising efficient algorithms for finding the ground state of molecular Hamiltonians. Some of the major approaches [5] include variational quantum eigensolver (VQE) [6–9], quantum phase estimation (QPE) [10–13], quantum imaginary-time evolution (QITE) [14–18], and quantum power iteration method [19,20].

Among these approaches, variational algorithms have attracted much recent attention with their potential to prepare the ground state of a complex Hamiltonian with a shallow quantum circuit in the noisy intermediate-scale quantum (NISQ) era. However, the hybrid quantum-classical optimization loop of the variational algorithms has soon been

pointed out to suffer a few prominent technical challenges. More specifically, the classical optimization not only faces a plethora of local minima but also may encounter notorious barren plateau [21–25] on the energy landscape. One possible scheme to mitigate this challenge is to simulate the QITE with the time-dependent variational principle. The variational simulation of the QITE avoids a deep quantum circuit and principally alleviates issues with optimizations, such as the barren plateau and local minimums [16].

Apart from the QITE, another common strategy to prepare a ground state by utilizing the time-dependent Schrödinger's function is adiabatic evolution in the real-time domain. Going beyond the adiabatic regime, the theory of optimal quantum control [26–29] provides a general tool and foundation for designing pulses to drive the desired state transitions in a finite time and in the presence of other constraints. Recently, the theory of Lyapunov quantum control has been used, in the context of hybrid quantum-classical algorithms, to solve classical optimization problems [30]. Under this formulation, one encodes the solutions to an optimization problem as the ground states of a classical spin system. To prepare a ground state, one temporally modulates the structural form of a Hamiltonian, via pulse engineering, in order to achieve the desired state-to-state transition. With the Lyapunov control theory, one can simply use the system's energy as the Lyapunov function to guide pulse engineering. Through our demonstrative examples below, the control-theory-inspired variational methods clearly exhibit faster convergence as well as enhanced robustness against noises compared to the standard VQE. Despite these encouraging instances, real-time

*yuqinchen@tencent.com

†alicehu@cityu.edu.hk

‡kimhsieh2@gmail.com

Published by the American Physical Society under the terms of the [Creative Commons Attribution 4.0 International](https://creativecommons.org/licenses/by/4.0/) license. Further distribution of this work must maintain attribution to the author(s) and the published article's title, journal citation, and DOI.

quantum control has hardly been regarded as a practical approach to prepare the ground state of strongly correlated many-body systems, because real-time control requires a careful analysis of the controllability of a given setup which is prohibitive to perform for complex systems [31,32]. Without full controllability, one cannot successfully steer a quantum system toward a target state as illustrated in our numerical example presented later in the text.

Using a temporally modulated Hamiltonian to steer many-body quantum dynamics is not restricted to the real-time domain. In fact, an extensive body of literature proposed quantum simulation methods involving complex time variables. Specifically, there is found that a QITE under the alternating influences of two different Hamiltonians may accelerate the convergence of the ground-state preparation problems [17]. The combination of interesting observations on the accelerated convergence of an open-loop control of a many-body QITE and the real-time control-based variational methods for shallow quantum circuits provoke more thoughts on whether one can efficiently prepare ground states based on a close-loop control theory for shallow parametrized quantum circuits in the imaginary-time domain.

We propose an imaginary-time Lyapunov control theory for ground-state preparation in this work. First, we theoretically discuss how steered Hamiltonian can speed up the ground state convergence. Then, we show a proper QITC can converge to the ground state faster than a QITE. For small-gap systems [33] such as examples on molecules reported in this work, we showcase that a QITC can even converge orders of magnitude faster than the standard QITE, suggesting an order-of-magnitude acceleration. Secondly, we discuss the essential differences between the real- and imaginary-time control theory. For the ground-state preparations, the quantum imaginary-time control (QITC) generally admits more lenient conditions on selecting control Hamiltonian to facilitate a given state transition. Thirdly, to make this method compatible with the limitation of the NISQ hardware, we formulate a time-dependent variational simulation of the QITC. Hence, one derives a new set of equations for time-dependent updates of parameters for an ansatz circuit. Finally, we test various systems like the diatomic molecules, 2D Heisenberg model, Sherrington-Kirkpatrick model, and a spin model constructed from a 3-SAT annealing problem [34] to ensure the existence of the speedup is general among many different cases. In addition, through numerical examples, we also demonstrate that the newly proposed variational version of the QITC not only converges faster than the standard variational QITE but also manifests higher robustness against noises of moderate strength. With a properly chosen set of control Hamiltonians, the variational simulation of the QITC does not incur many measurement overheads. For instance, if one chooses H_d that commutes with the constituting Pauli terms in H_p , then one can significantly minimize the number of measurement overheads.

II. THEORETICAL MOTIVATION

A time-dependent Hamiltonian in the imaginary-time domain is given by

$$\frac{d\psi(\tau)}{d\tau} = -(H_p - E_\tau)\psi(\tau), \quad (1)$$

where $\psi(\tau)$ is the system's state vector, H_p is the problem Hamiltonian, and $E_\tau = \langle \psi(\tau) | H_p | \psi(\tau) \rangle$ is the state's expected energy, and it is introduced in Eq. (1) to ensure the time-evolved wave function will be properly normalized. By eigendecomposition, we can write the problem Hamiltonian H_p as $H_p = U \Lambda U^\dagger$, where U is a unitary matrix and $\Lambda = \text{diag}(\lambda_0, \dots, \lambda_n)$ is a diagonal matrix where $\lambda_0 \leq \lambda_1 \leq \dots \leq \lambda_n$. Consider an additional Hamiltonian H_d that commutes with H_p and follows the same ordering of eigenstate in energy then,

$$H_d = U D U^\dagger, \quad (2)$$

where $D = \text{diag}(e_0, \dots, e_n)$ is a diagonal matrix with $e_0 \leq e_1 \leq \dots \leq e_n$. The energy difference between the ground state and the i th eigenstate will change from $\Delta_{i0} = \lambda_i - \lambda_0$ to $\tilde{\Delta}_{i0} = \Delta_{i0} + (e_i - e_0)$. Since the extra contribution to the energy gap $\delta_{i0} = e_i - e_0 > 0$ for all δ_{i0} , the imaginary-time evolution under $H_p + H_d$ will then be greatly accelerated [proportional to $\exp(\delta_{i0})$] in comparison to the time evolution under H_p alone. Through simple arguments, we illustrate a sufficient (but not necessary) condition that may yield the ideally great speedup on the imaginary-time evolution by imposing an additional Hamiltonian H_d that commutes with H_p and preserve the ordering of eigenstates of H_p by energy. Even though it is computationally prohibitive to construct H_d when the Hilbert space is large [19], the revelation in this theoretical analysis provides a clear direction to proceed. We carefully discuss a series of practical approximations attempting to gain speedup in the imaginary-time evolution. For all the simulation experiments in the paper, the construction of control Hamiltonian follows the approximation methods. We also denote that following the control strategy involving maximum admissible control impulses assists to ensure the substantial acceleration effect.

III. QUANTUM IMAGINARY TIME CONTROL

A quantum system's dynamical evolution under a time-dependent Hamiltonian in the imaginary-time domain is given by the modified time-dependent Schrodinger's equation,

$$\frac{d\psi(\tau)}{d\tau} = -(H_p + \beta(\tau)H_d - E_\tau)\psi(\tau), \quad (3)$$

where $\psi(\tau)$ is the system's state vector, H_p is the problem Hamiltonian, and H_d is the control Hamiltonian coupled to a time-dependent control pulse $\beta(\tau)$. $E_\tau = \langle \psi(\tau) | (H_p + \beta(\tau)H_d) | \psi(\tau) \rangle$ is the state's expected energy, and it is introduced in Eq. (3) to ensure the time-evolved wave function will be properly normalized. According to the Lyapunov method and La Salle invariance principle [35], the state preparation problem can be re-formulated as an optimization problem in which the target state minimizes a Lyapunov function $V(\psi(\tau))$, which must satisfy the following conditions. Consider a system of differential equations $\dot{\psi}(\tau) = f(\psi(\tau))$ with a smooth f and the state of the system satisfies the conservation of probability $\|\psi(\tau)\| = 1, \forall \tau \geq 0$, which means that ψ is on the unit sphere $\mathbf{S} = \{x \in \mathbf{C}^n : \|x\| = 1\}$. Consider a smooth function $V(\psi)$ on the phase space Ω , such that $V(\psi) \geq 0$ and $\frac{dV(\psi)}{d\tau} \leq 0$ for $\psi \in \Omega$. Let us define \mathcal{M} to be the set of points $\psi \in \Omega$ such that $dV(\psi)/d\tau = 0$, then every

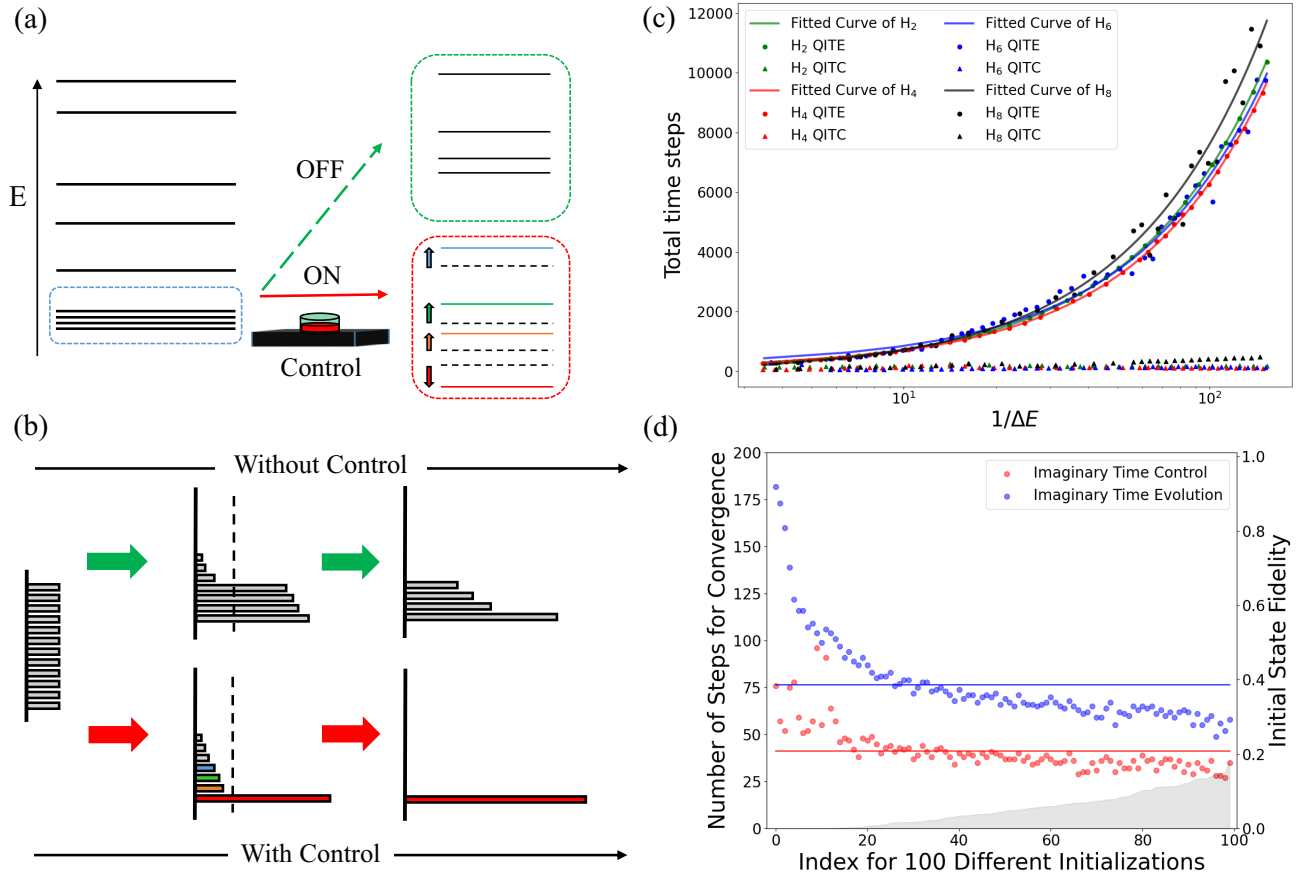


FIG. 1. (a) A temporally modulated Hamiltonian to steer many-body quantum dynamics. (b) The QITE gets slowed down significantly when the current state is the combination of many low-energy eigenstates. (c) The H-chain results for even hydrogens that are scaled from H_2 to H_8 . The dots of different colors indicate the total convergence steps of QITE and QITC in different systems, and lines of different colors indicate that the fitted curves of QITE satisfy $f(x) = ae^x + b$, where $x = \log(1/\Delta E)$. On the other hand, the QITC results yielded $f(x) = ax + b$. (See the details in Appendix B1.) (d) The numerical results of four qubits H_2 molecule with bond length 0.74 and 100 random initial state, the x axis is the case number we assign for randomly chosen initial points, the left y axis is the number of convergence, and the right y axis is the state fidelity between the initial state and ground state. The control Hamiltonian used here is single Pauli Z.

solution of the time-dependent Schrodinger's equation converges to \mathcal{M} as $t \rightarrow \infty$.

For the preparation of the ground state of a Hamiltonian, the Lyapunov function can be chosen as follows:

$$V(\psi(\tau)) = \langle \psi(\tau) | P | \psi(\tau) \rangle, \quad (4)$$

where $P = H_p - \tilde{E}$ with \tilde{E} a constant shift of energy to ensure that P is a semipositive definite Hermitian operator [36]. The time derivative of the Lyapunov function in Eq. (4) reads

$$\dot{V}(\psi) = 2\sigma_{H_p}^2(\tau) - \beta(\tau)D(\tau), \quad (5)$$

where ψ is an abbreviation for $\psi(\tau)$. The other variables are given by

$$\begin{aligned} \sigma_{H_p}^2(\tau) &\equiv \langle \psi | H_p | \psi \rangle^2 - \langle \psi | H_p^2 | \psi \rangle, \\ T(\tau) &\equiv \langle \psi | \{H_p, H_d\} | \psi \rangle - 2\langle \psi | H_p | \psi \rangle \langle \psi | H_d | \psi \rangle, \end{aligned} \quad (6)$$

where $\{\cdot, \cdot\}$ is the anticommutator. In this case, the Lyapunov-controlled quantum dynamics will be driven to the asymptotically stable points, which form the ground-state manifold, in \mathcal{M} . To make $\dot{V}(\psi) \leq 0$, it is sufficient to enforce $\beta(\tau)T(\tau) \geq$

0 as $\sigma_{H_p}^2(\tau)$ is less than or equal to zero. In summary, a successful imaginary-time control to prepare the ground state of a Hamiltonian is to design an appropriate $\beta(\tau)$ and suitable H_d (see Appendix A). For this work, we proposed some control strategies (see Method) that are inspired by the bang-bang and approximate bang-bang Lyapunov control that can provide rapid state transitions for quantum systems in the real-time domain [37].

A. Comparison to imaginary-time evolution

We find that QITE gets slowed down significantly when the current state is mainly a superposition of many densely spaced low-energy eigenstates Fig. 1(b). For the original H_p the energy gap between the ground state and the first excited state remains fixed and limits the simulation efficiency. Consistent with the theoretical motivation stated before, we find that the QITC temporally modulates the entire spectrum of $H(\tau)$ during the evolution and finally returns back to the original spectrum of H_p . Those temporally enlarged energy

gaps contribute to the acceleration of the simulation process, see Fig. 1(a)

In Fig. 1(c), we present the results of ground-state preparation, it shows that the QITC provides orders of magnitude speedup (suggesting order-of-magnitude acceleration) in the rate of convergence with respect to the intra-molecular distance. Note that the Δ_{10} energy gap reduces when the intra-molecular distance grows. This observed scaling trend certainly benefits the simulation of large complex systems with small energy gaps. To ensure this observed significant speedup holds in a variety of chemical systems, we provide simulation results of four, eight, twelve, and sixteen-qubit hydrogen chains, a twelve-qubit LiH, and HF in the following section. In Fig. 1(d), we illustrate the enhanced convergence efficiency for the QITC with different initial states. These results also indicate that the convergence of the QITC does not sensitively depend on the initial states.

B. Comparison to the real-time control for the ground-state preparation

An essential question for a driven state preparation concerns the controllability for the given control Hamiltonians $\{H_d^0, H_d^1, \dots\}$, i.e., whether the quantum system can be driven to the ground state of H_p from any given initial state when it is subjected to evolve under the time-dependent Hamiltonian $H(\tau) = H_p + \beta(\tau)H_d$ in our context, where $H_d = \sum_i \beta^i(\tau)H_d^i$. Without loss of generality, we write $\beta(\tau)H_d$ as opposed to the more general form $\sum_i \beta^i(\tau)H_d^i$ throughout this work. This simple question for real-time control turns out to be rather difficult to answer for a large quantum system. A common technique involves analysis of the structure and rank of corresponding Lie groups and algebra for the propagators [38–40]. It is computationally demanding to determine the controllability of a particular setup, and it is unlikely that a random selection of control Hamiltonians can guarantee complete controllability. The challenge to select an appropriate set of control Hamiltonians (with respect to a given initial state) poses a severe challenge to derive a practical real-time control strategy to prepare a target ground state.

The same question regarding controllability admits a much clearer answer in the imaginary-time domain. As long as the imaginary-time-evolved state $\psi(\tau)$ and the ground state have a nonzero overlap, the system can always converge to the ground state in a sufficiently long evolution time. Hence, a more crucial question is whether a set of control Hamiltonians along with the corresponding control strategy $\beta(\tau)$ [i.e., to ensure $\dot{V}(\psi) \leq 0$] can substantially accelerate the driving from a given initial state to the ground state of H_p . As discussed next, the imaginary-time Lyapunov control can indeed work with a broader range of control Hamiltonians for accelerating the ground-state preparations.

We further illustrate the differences between real-time and imaginary-time Lyapunov control with a numerical example involving H_2 molecule in Fig. 2. We randomly choose 100 initial states and examine how long the real-time and imaginary-time evolutions converge to the ground state under control Hamiltonians with various degrees of controllability. When the control Hamiltonian satisfies the strongly complete

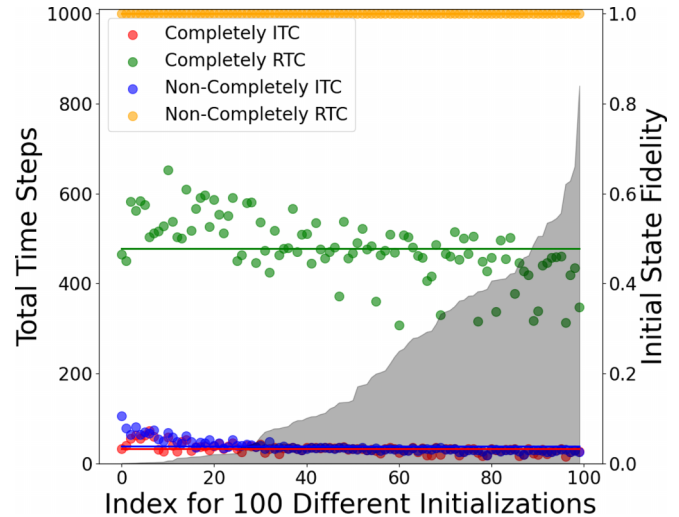


FIG. 2. The numerical result of 2 qubits H_2 molecule (see Appendix D), the x axis is a serial number of initial states, the left y axis is the convergent steps, the maximum number of steps is limited to 1000, and the right y axis (corresponding to the grey area) is the initial and ground state overlap. The complete imaginary-time control (completely ITC (red)), the noncompletely imaginary-time control (noncompletely ITC (blue)), and the complete real-time control [completely RTC (green)] could all converge in time. However, the noncompletely real-time control [noncompletely RTC (yellow)] cannot converge in a limited time.

controllability [41], we expect that the driven dynamics converge to the ground state without difficulty. While this expectation holds in the numerical experiments, we find the imaginary-time evolution converges much faster (with roughly one-tenth of the time steps for the real-time evolution on average). We expect this performance gap to be further enlarged with the system size. For control Hamiltonians with incomplete controllability, the imaginary-time control can still lead to satisfactory convergence in a small number of time steps. In contrast, the real-time simulation under the same control Hamiltonians cannot converge for all 100 initial states in the predefined maximum number of steps allowed.

C. Comparing QITC and VQE in noisy environment

To make the method accessible in the noisy intermediate-scale quantum era, we further propose a variational form of the algorithm that could work with shallow quantum circuits. To utilize the proposed imaginary-time control to prepare a ground state on a near-term quantum device, we rely on the time-dependent variational principle to approximate the evolution of the QITC as sequential updates of parameters for an ansatz circuit, as first proposed by McArdle *et al.* [16], for the QITE. The modified algorithm proceeds as follows. Given a time-dependent Hamiltonian $H(\tau) = H_p + \beta(\tau)H_d$, we would invoke the McLachlan’s variational principle [42,43],

$$\delta \|(\partial/\partial\tau + H(\tau) - E_\tau)|\psi(\tau)\| = 0, \quad (7)$$

which conducting the dynamic evolution $\partial|\psi(\tau)\rangle/\partial\tau = -[H(\tau) - E_\tau]|\psi(\tau)\rangle$ by deducing the incremental update

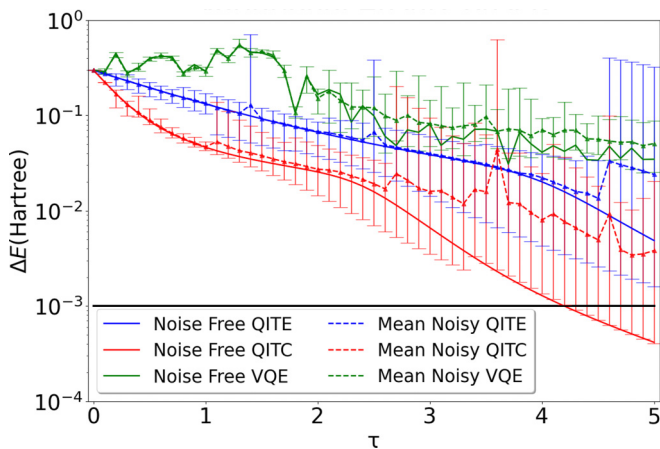


FIG. 3. The numerical results of four-qubit hydrogen molecule (see Appendix D) with a bond length of 0.74 \AA on the noisy device. The x axis is imaginary time with a single time step $\Delta\tau = 0.1$ and the total time step is 50. The y axis is the energy difference from ground-state energy. The solid line is the result of the numerical noise-free model (the black line is chemical accuracy). The numerical noisy model is simulated by adding the single qubit depolarization error channels with parameter $\lambda = 10^{-4}$ and the CNOT depolarization error channels with parameter $\lambda = 10^{-5}$ (we use TENSORCIRCUIT [44] to effectively get this result). The dashed line is the mean value of 50 noisy results, and the error bar is bounded by the worst and best simulation results. The control strategy used in this simulation is approximately bang-bang control with $S = 0.3$ and $\gamma = 5$.

(corresponding to one time step $\delta\tau$) of the parameters θ for an ansatz circuit. Following Ref. [16], we need to solve the following equations:

$$\sum_j A_{ij}\dot{\theta}_j = C_i, \forall i; \quad (8)$$

where

$$A_{ij} = \Re\left(\frac{\partial\langle\phi(\tau)|}{\partial\theta_i} \frac{\partial|\phi(\tau)\rangle}{\partial\theta_j}\right),$$

$$C_i = \Re\left(-\sum_\alpha \lambda_\alpha \frac{\partial\langle\phi(\tau)|}{\partial\theta_i} h_\alpha |\phi(\tau)\rangle\right), \quad (9)$$

and h_α and λ_α are the Pauli terms and coefficients of the Hamiltonian $H = H_p + \beta(\tau)H_d = \sum_\alpha \lambda_\alpha(\tau)h_\alpha$. With the new ansatz state, we can then evaluate the Lyapunov function and assign values to the pulse $\beta(\tau)$ via a predetermined control rule to keep $\dot{V}(\psi) < 0$. The procedure of alternating updates of θ and β is then repeated until a fixed point is reached. In this section, we compare the simulation ability of VQE, variational imaginary-time evolution, and variational imaginary-time control. In Fig. 3, we compare the results among the VQE, the variational ansatz-based QITE, and the variational ansatz-based QITC for the ground-state preparation of a four-qubit H_2 system under both noise-free and noisy situations. We adopt the fully connected ansatz with high expressibility [45] initialized by the same random initial parameters for all the methods. The results show that the QITC converges faster than the QITE and the VQE for both the noisy and noise-free models. The control Hamiltonian we

TABLE I. The result of 2D Heisenberg model. The $(2 \times 2)_D$ is the “difficult” regime in the space of Hamiltonian parameters case where QITE required a great number of steps to converge. All the control Hamiltonians are in the structure of simple Pauli Z with the cyclic structure mentioned above and we only write down the nontrivial part of Pauli in the table. For example, the ZIZ in the 22 model is the abbreviation of ZIZIIIII. The number of control steps for all cases is 100 steps.

Model	(1×1)	(2×2)	(3×3)	(2×2) _D
h/J	0.1/0.09	0.1/0.09	0.1/0.09	0.2/0.1
QITE total time step	366	764	5963	28 934
QITC total time step	130	253	1137	182
Difference	236	511	4826	28752
Ratio	2.82	3.02	5.24	158.98
Control	ZIIZ	ZIIZ	ZIIZ	ZIIZ
Hamiltonian (H_d)		ZIZ	ZZZ	ZZZ
Number of H_d	4	18	32	18

using here is the single Z and double Z selected from the hydrogen Hamiltonian H_p .

IV. EXAMPLES BEYOND H CHAINS

First, we simulate two diatomic molecules HF and LiH to test the speedup from the control in molecule systems. In Figs. 4(a) and 4(b), we show that both the HF and LiH using the same control Hamiltonian used in the H-chain system can obtain order-of-magnitude speedup. Second, we consider a spin model constructed from the annealing solving of an 11-qubit 3-SAT problem during the linear schedule, see $H(s)$ defined in Appendix B3. We then implement and compare the simulations of the ITC and the ITE in order to prepare the ground states for a series of $H(s)$ chosen along the adiabatic path. According to the simulation result in Fig. 4(c), we numerically verify the speed-up of the ITC as the instantaneous energy gap $\Delta E(s)$ shrinks. Third, we demonstrate the 2D Heisenberg model (see Hamiltonian details in the Method section) with different system sizes using control Hamiltonian constructed only by Pauli Z up to cube order. As we can see from the results in Table I, Lyapunov control provides obvious speed-up while the system size scales up. The $(2 \times 2)_D$ case also indicates the existence of great speed-up using simple control Hamiltonian Pauli Z.

Finally, we simulate a four-qubit variational-ansatz based imaginary-time evolution of the spin glass model (see Hamiltonian details in the Method section) in Fig. 5 with random variables $J_{ij} = (0.049, 0.215, 0.103, 0.045, -0.076, 0.146)$, the energy difference between the ground state and first excited state Δ_{10} , in this case, is 0.22 which is not small compared to the result of our molecule models. Although the QITE can work fine with such Δ_{10} , it is still difficult to find a good initial state for a complex system like this SK model. To prepare a better initial state, we use VQE with COBYLA optimizer and variational QITC with commute basis $H_d = \{XXXX, YYYY, ZZZZ\}$ at the first ten steps, respectively. After the initial state preparation, we use variational imaginary-time evolution to evolve to the ground state given these two initial states. It can be seen that compared

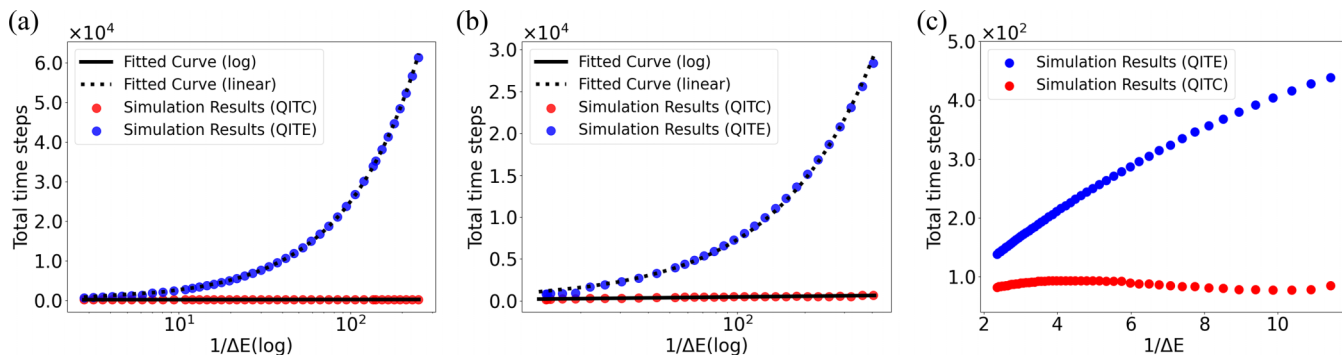


FIG. 4. (a) The numerical result of 12 qubits HF molecule (see Appendix D) with bond length from 1.00 to 2.36 Å and the same initial state with equal superposition of all the basis states, the QITE is the result of imaginary-time evolution. The QITC is the result of the imaginary-time control, the x axis refers to the log of one over the energy gap between the ground state and the first excited state, and the y axis is the total time step. QITE fitted curve $f(x) = 248.67 \exp(x) + 126.12$ and QITC fitted curve $f(x) = 12.80x + 110.09$, where $x = \ln(1/\Delta E)$. (b) The numerical result of 12 qubits LiH molecule (see Appendix D) with bond length from 2.00 to 4.00. The x axis is log of one over energy gap between the ground state and the first excited state. The y axis is the total time steps of the QITE and QITC. QITE fitted function $f(x) = 71.60 \exp(x) + 154.96$ and QITC fitted curve $f(x) = 125.31x - 108.81$, where $x = \ln(1/\Delta E)$. (c) The result of 3-SAT quantum annealing problem (see Appendix B). The x axis is the one over the energy gap between the ground state and the first excited state. The y axis is the converge steps difference between the QITE and QITC.

with the VQE initial state, the control initial state can achieve higher accuracy under the same number of convergence steps. The details and more discussion of the models are presented in Appendix B.

V. RESOURCE CONSUMPTION FOR SCALING H-CHAIN SYSTEM

So far, we have only discussed the conceptual advantage of our method (i.e., faster convergence towards the ground state). As we propose this method in the context of digital quantum simulation on a quantum computer, we further analyze how our method helps to reduce the consumption of quantum resources. Here we present the number of measurements for H_2 , H_4 , H_6 and H_8 (i.e., 4, 8, 12, and 16 qubits)). In Fig. 6, we summarize this reduction in the number of measurements

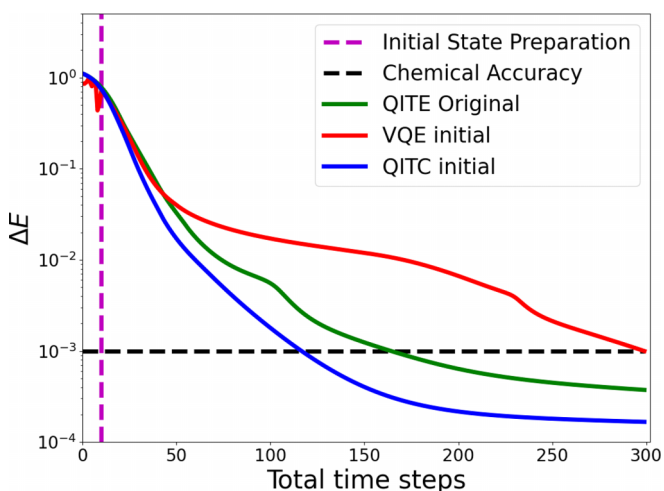


FIG. 5. The result of 4 qubits SK model with different initial-ization. The x axis is the number of time steps and the y axis is the energy difference from the ground state. The control initial can achieve chemical accuracy around three times faster than the VQE initial with a smoother convergence path.

with different choices of H_d (see Appendix B for details): The Full H_d with the same $1/\Delta E$ (blue bar), the Half H_d with same $1/\Delta E$ (orange bar), the Full H_d with the same bond length(green bar) and the Half H_d with the same bond length(red bar). The result shows that all of them give some polynomial reductions in the number of measurements, compared to the standard variational ansatz-based imaginary-time evolution. This is because the extra measurement numbers from H_d, H_p are relatively small in comparison to the variational ansatz update measurements, which scales as $N_p N_\theta$, where N_p is the number of Pauli terms of H_p and N_θ is the number of the parameter in the ansatz circuit (we used

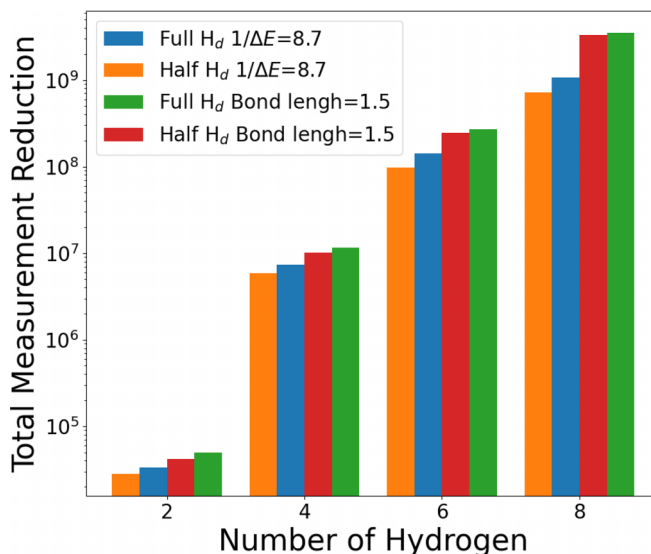


FIG. 6. Total measurement difference results. The results are the estimation of the difference in total measurements for imaginary-time evolution and imaginary-time control convergence, the calculation details are listed in Table II. The x axis is the number of H in the system and the y axis is the log plot of the measurement reduction. The full H_d and half H_d are listed in Appendix B.

TABLE II. Summary of Measurement test, where N_p is the number of Pauli terms of problem Hamiltonian H_p (here we use Jordan-Wigner transformation), N_θ is the number of parameters in the ansatz circuit (here we use k-UpCCGSD) and $N_p N_\theta$ is the number of measurement to update the variational-ansatz based imaginary-time evolution. $\{H_p, H_d\}$ is the extra measurement for update control Hamiltonian coefficient $\beta(\tau)$ and ΔStep are the total time step difference between imaginary-time evolution and imaginary-time control. The ΔStep_f and ΔStep_h are the total time step difference using Full H_d control and Half H_d control for same bond length case.

	N_p	N_θ k-UpCCGSD	$N_p N_\theta$	Full H_d		Half H_d		Same bond length	
				$\{H_d, H_p\}$	ΔStep	$\{H_d, H_p\}$	ΔStep	ΔStep_f	ΔStep_h
H_2	15	6 ($k = 1$)	90	5	381	5	327	554	473
H_4	185	72 ($k = 2$)	13 320	1006	555	577	449	872	771
H_6	919	270 ($k = 3$)	248 130	16 627	572	8804	399	1098	991
H_8	2913	672 ($k = 4$)	1 957 536	112 396	544	57 966	377	1804	1712

k-UpCCGSD from PennyLane for the reference). In Table II, we show the N_p , N_θ , and extra measurements for different H_d . Thus according to Fig. 6, for the molecules tested in this study, we find the measurement resource reduction increases polynomially with the system size.

VI. THE IMAGINARY TIME CONTROL STRATEGY

In this section, we will discuss the approximate bang-bang control and bang-bang control laws we use to design the $\beta(\tau)$ for imaginary-time control and the inverse control strategy we used to accelerate our molecule system ground state convergence. To appreciate our approach, we first review some typical real-time control strategies designed to guarantee $\dot{V} \leq 0$. Following a standard convention [37], we refer to the following choice as the standard Lyapunov control:

$$\beta_k(t) = -K_k T_k(t),$$

where $\beta_k(t)$ is an external real-valued control field, $K > 0$ is the control gain used to adjust the amplitude of the control field, and $T_k(t) \equiv (\langle \psi | i[H_d, H_p] | \psi \rangle)$ for the real-time control. Another commonly used strategy is the bang-bang Lyapunov control,

$$\beta_k(t) = \begin{cases} -S, & (T_k > 0) \\ S, & (T_k < 0) \\ 0, & (T_k = 0) \end{cases} \quad k = 1, \dots, m,$$

where $S > 0$ is the maximum strength of the control field. In order to achieve a good trade-off between convergence and the rapidity of control, Kuang *et al.* [37] propose an approximate bang-bang control as follows:

$$\beta_k(t) = \frac{2S}{1 + e^{-\gamma T_k}} - S.$$

where $\gamma > 0$ is a parameter used to adjust the hardness of the control strategy. For the imaginary-time control strategy, let us generalize the standard Lyapunov control such that it could work with the imaginary-time evolution. We redefine $T_k \equiv 2\langle \psi | H_p | \psi \rangle \langle \psi | H_d | \psi \rangle - \langle \psi | \{H_p, H_d\} | \psi \rangle$ in this case. The H_d related terms in $T_k(\tau)$ may entail lots of extra measurements if they cannot be obtained by measuring the Pauli terms appearing in $\langle \psi | H_p | \psi \rangle$. To reduce the measurement cost and still maintain a powerful H_d to provide an enhanced convergence, we propose the following strategy. We first decide if the state in the quantum circuit has high overlap with any eigenstate of

H_p or H_d by checking the value of T_k , if $T_k < L$ then we do not apply any control pulses, otherwise we use a similar control strategy for the real-time case introduced above.

$$\beta_k(\tau) = \begin{cases} \frac{2S}{1 + e^{-\gamma T_k}} - S, & T_k \geq L \\ 0, & \text{else} \end{cases},$$

where L is some predefined threshold value. If the state is close to an eigenstate [i.e., $T_k(\tau) < L$], we should turn off the control field and let the system evolves under H_p in the imaginary-time domain. This truncation can greatly reduce the measurement costs (for the implementation of the corresponding variational algorithm) in the region where the state will linearly converge to the eigenstate. Finally, we test how the truncation [i.e., setting $\beta_k(\tau) = 0$ when $T_k(\tau) < L$] will affect the precision of the converged results given by truncating the control pulse, and we also test the control with different phases in Appendix C.

VII. DISCUSSION

In summary, we propose to utilize the imaginary-time Lyapunov control to prepare ground states and explain the advantages of QITC. First, imaginary-time control can speed up imaginary-time evolution with the proper design of control Hamiltonian and control function $\beta(\tau)$. Through numerical experiments on a broad spectrum of realistic models, we show that compared to standard imaginary-time evolution, imaginary-time control provides substantial speed-up for all systems. And for the selected small-gap systems invested in this work, an order-of-magnitude speedup is observed. Secondly, compared to real-time control, imaginary-time control admits more relaxed conditions for controllability (when the target is the ground state) and a broader range of control Hamiltonians to facilitate the desired state transitions in a finite time. Thirdly, to make the present method accessible in the NISQ era, we propose a variational simulation of the QITC with an ansatz circuit. Finally, we show various examples to strengthen the speedup from QITC. We also show that when the control Hamiltonian is chosen appropriately, it does not incur many additional measurement costs and exhibits higher robustness against noises. These merits make the present approach a natural replacement for the variational ground-state preparation. For future work, we aim to study imaginary-time control for other challenging state preparation tasks, such as excited states simulation and Gibbs state preparation, etc.

ACKNOWLEDGMENTS

A.H. gratefully acknowledges the sponsorship from the City University of Hong Kong (Project No. 7005615); and the Hong Kong Institute for Advanced Study, City University of Hong Kong (Project No. 9360157). The work described in this paper was substantially supported by a grant from the Research Grants Council of the Hong Kong Special Administrative Region, China (Project No. CityU 11200120).

APPENDIX A: ACCELERATION INDUCED BY LYAPUNOV CONTROL

In this section, we explain the simulation acceleration driven by Lyapunov control in multiple stages. First, we discuss a practical strategy to construct a control Hamiltonian (without explicitly diagonalizing the system Hamiltonian) that ensures substantial speedup in Sec. A 1. Second, we attempt to provide an intuitive understanding of the accelerated dynamical process by inspecting time-dependent changes in the distribution of eigenstate populations and the time-evolved energy spectrum of $H(\tau)$ in Sec. A 2. In Sec. B, we look at a broad spectrum of realistic models (of interest in condensed matter physics, quantum chemistry, and combinatorial optimization) to demonstrate the broad applicability of the proposed method for simulating the ground state of a Hamiltonian.

1. General strategy for control Hamiltonian construction

As stated in the previous section, one scenario to drive the ideally-great speedup is to construct an H_d that (1) commutes with H_p , (2) maintains the eigenstate ordering of H_p and (3) holds the matrix norm for $H_p + H_d$ roughly the same as that of H_p . Among the three criteria, it is reasonable to partially relax the condition on the eigenstate ordering and make $H_d(t)$ a time-dependent control Hamiltonian instead.

One possibility is to choose $H_d(t) = \sum_{i=1}^n \beta_i(t) H_p^i$, which is an n -th order matrix polynomial made up of power of H_p^i and $\beta_i \in \mathbf{R}$. Intuitively, the time-dependent spectrum of $H_d(t)$ may temporarily alter eigenstate ordering and enlarge or shrink energy gaps between states. Under this temporal modulation of the Hamiltonian spectrum, there would be accelerated and de-accelerated population transfer among eigenstates of H_p during the imaginary-time evolution. To ensure that we obtain as large an energy filtering towards the ground state of H_p as possible is to simply minimize the expected energy value $\langle \psi(t) | H_p | \psi(t) \rangle$ during the imaginary-time evolution under $H_p + H_d(t)$. The gradient descent will give us the rule to update $\beta(t)$. At this point, this strategy of optimizing $H_d(t)$ essentially corresponds to the closed-loop control theory discussed thoroughly in the main text.

We now have a simple and clear picture for the selection of control Hamiltonian. However, it might not be experimentally feasible to implement such a complex form of control Hamiltonian, $H_d(t) = \sum_{i=1}^n \beta_i(t) H_p^i$. An approximate option is to retain only the major components of H_p in this polynomial expansion of $H_d(t)$. Effectively, instead of having an $H_d(t)$ that always commutes with H_p , we end up considering an $\tilde{H}_d(t)$ with nonzero off-diagonal matrix elements in the eigenbasis of H_p . While this compromise (due to realistic experimental

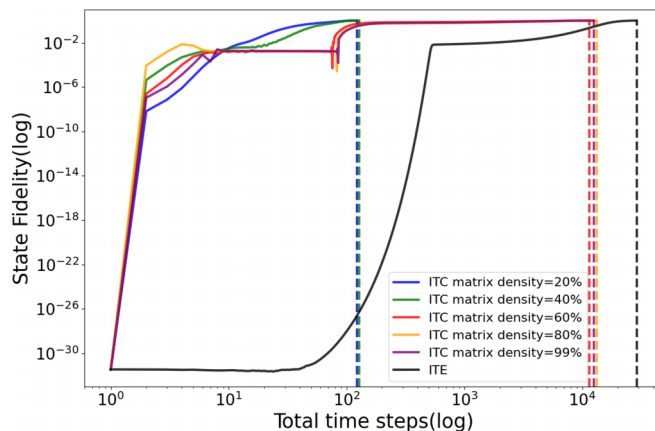


FIG. 7. The convergence results of H_d . The ITC matrix density is the percentage of the matrix \tilde{D} filled with the nonzero number range from 0 to 1. The x axis is the logarithm of the total convergence time step. The y axis is the fidelity between the convergence state and the ground state.

constraints) may offset the ideally-great speedup, we find that it is still possible to achieve an appreciable speedup within the closed-loop control setup. To make the discussion in this section self-contained, we present a numerical illustration.

In Fig. 7, we show the simulation result of how the imperfectly controlled dynamics, driven by $H_p + \tilde{H}_d(t) = U\tilde{D}(t)U^\dagger$, affect the convergence of imaginary-time evolution for a 9 qubits 2D XXX model with nonperiodic boundary condition. The problem Hamiltonian can be written as $H_p = 0.2 \sum_i Z^i + 0.1 \sum_{\text{edge}} X^i X^j + Y^i Y^j + Z^i Z^j$, where edge implies the nearest-neighbor couplings and the initial state is $|+\dots+\rangle$. Assume that the originally intended control Hamiltonian H_d is intended to enlarge the energy gaps between the ground state and excited states, but, due to the experimental constraints, we choose to adopt a more easily implementable \tilde{H}_d . In this case, we no longer have a fully diagonal matrix D in the eigenbasis of H_p rather we consider

$$\tilde{D} = \begin{pmatrix} -5 & 0 & 0 & \dots \\ 0 & 0 & 0 & \dots \\ \dots & \dots & \dots & \dots \\ 0 & 0 & 0 & 0 \end{pmatrix} + \mathcal{R}(p),$$

where $\mathcal{R}(p)$ is a random sparse matrix with p percentage of nonzero off-diagonal matrix elements. The result shows that the H_d with nontrivial off-diagonal disorder ($\tilde{D}(p = 20\%$ and $p = 40\%$) can still maintain the ideally-great speedup (approximately approach exponential speedup) for this problem, although the further increase of the number of off-diagonal terms will eventually suppress the speedup. Interestingly, when the number of nonzero off-diagonal disorders rises up to $p = 60\%$ the inhibition effects on the speedup of this nine-qubit system seem to plateau.

In a practical scenario, the control Hamiltonian for the models in Appendix B follows the rules we mentioned above. For molecular systems studied, Pauli Z terms are the dominant terms in H_p with large coefficients. The selection of those dominant Pauli Z terms as control Hamiltonian follows the rule (1) since it commutes with the highest contribute terms in

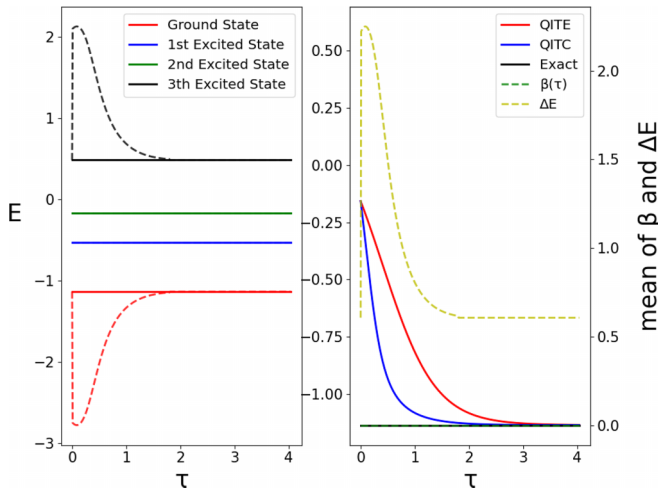


FIG. 8. The result of two-qubit hydrogen with complete control. The left figure shows how the energy levels change with time, as the solid line is the original energy level and the dashed line is the controlled energy level. The right figure is the convergence of imaginary-time models. The left y axis corresponds to the energy for the red solid and blue solid lines. The right y axis corresponds to the energy gap between the ground state and the first excited state, and the $\beta(\tau) = \frac{1}{n} \sum_{i=1}^n \beta_i(\tau)$. The result shows that all energy levels will change with time.

H_p therefore approximately commutes with H_p . The details of H_d selection are listed in Appendix B 1. For complex systems like the XXX model and SK model, Pauli Z terms from H_p may not be dominant parts. We select the k -local Pauli Z as H_d , which not only commutes with all Pauli Z terms but also commutes with many Pauli XX(YY) terms making it approximately follow the rule (1). Finally, proper design of the control strategy and maximum admissible control impulses will allow rules (2) and (3) to be successfully followed, see details in Appendix C.

2. Dynamic process visualization

We find the ITC temporally modulates the entire spectrum of $H(\tau)$ during the evolution and return back to the original spectrum of H_p when time $t \gg 1$ as $\beta(t \gg 1) \rightarrow 0$. As can see in the following figures, for the case of the imaginary-time evolution (ITE), since the H_p is a time-independent Hamiltonian, the energy gap between the ground state and the excited states remains fixed in time. For the imaginary-time control (ITC), on the other hand, the energy gap between the ground state and the excited states of H_p will change with time. However, unlike the polynomial basis that can guarantee to order of the whole eigenspectrum as in Fig. 8, the small set of limited Pauli basis might only modify some of the eigenstates as in Fig. 9. We comment on how the energy gap changes with time under control using different control Hamiltonians from the point of view of controllability, which provides another realization of how the control Hamiltonian orders the energy spectrum during the convergence. The idea is borrowed from the idea of controllability discussed in real-time control [41], in our definition, given a set of reachable states denoted by $\mathcal{R}(|\psi_0\rangle)$ start from initial

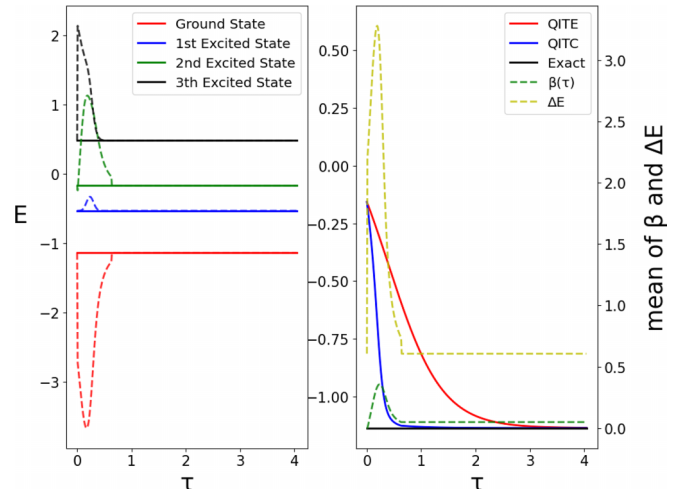


FIG. 9. The result of two-qubit hydrogen with noncomplete control shows that the highest excited state and the ground state will both change with time.

state $|\psi_0\rangle$, the control system $H_p + \beta(\tau)H_d$ is said to be completely (eigenstates) controllable if $\mathcal{R}(|\psi_0\rangle) = \mathcal{E}$, where \mathcal{E} is the collection of eigenstates, and said to be noncompletely (eigenstates) controllable if $\mathcal{R}(|\psi_0\rangle) \neq \mathcal{E}$. From the point of view of the energy spectrum, since the final convergence state of imaginary-time evolution should be the ground state of the new system, the control system should reorder the whole energy spectrum during the convergence when the control system is completely controllable. For the control system that is not completely controllable, it can still accelerate the ground state convergence if the ground state in the reachable state $\mathcal{R}(|\psi_0\rangle)$ which should always be true since ITC can switch back to the original ITE by the turn of the β . By definition, it is clear that polynomial basis is in the class of completely controllable, and limited Pauli basis might be in one of the classes according to the elements in the basis. In the following numerical experiment, we will visualize the concept of controllability using the energy spectrum. The energy gap between the ground state and the excited states of H_p will change with time as

$$\Delta E(\tau) = \langle \psi_0 | H(\tau) | \psi_0 \rangle - \langle \psi_i | H(\tau) | \psi_i \rangle.$$

where $H(\tau) = H_p + \beta(\tau)H_d$, $|\psi_0\rangle$ and $|\psi_i\rangle$ correspond to the ground state and i -th excited state of drift Hamiltonian H_p , respectively. In Fig. 8, we show the simulated result of using an ITC to prepare the ground state for a two-qubit hydrogen model. In this case, we adopt a set of control Hamiltonians that yield complete controllability (polynomial basis), on the two-qubit dynamics. As clearly illustrated in the figure, the ITC temporally modulates the entire spectrum of $H(\tau)$ during the evolution and returns back to the original spectrum of H_p when time $t \gg 1$ as $\beta(t \gg 1) \rightarrow 0$. Thus we conclude that the controlled system can evolve towards the ground state of H_p in fewer time steps with enlarged energy gaps.

Next, we attempt a different experiment. If the control Hamiltonian does not guarantee complete controllability (limited Pauli basis), the imaginary-time control will not be able to enlarge all energy gaps but just a few of them. In this case, it can still speed up the convergence of the ITC but may not

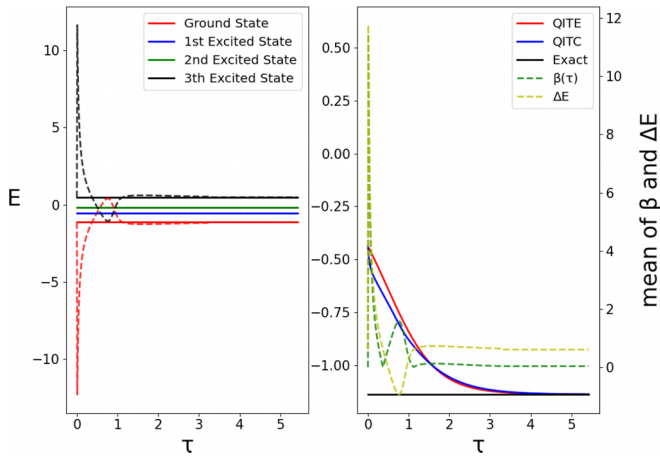


FIG. 10. The result of two-qubit hydrogen with aggressive control strategy shows that the control pulses are able to rearrange energy level.

be as fast as the previous case with complete controllability. In Fig. 9, the two-qubit hydrogen is driven by a noncomplete controllable Hamiltonian H_d , the instantaneous ground state energy drop increases the energy gap between the ground state and the excited states, therefore, provide the speed-up for ITC, and this control will benefit more when the initial state has an appreciable overlap with the highest excited state since the highest excited state is also controllable.

However, when the control Hamiltonian is not completely controllable and the control strategy $\beta(\tau)$ is too aggressive, then the driven ITE may actually compromise the rate of convergence. This is because the ground state has been inverted to the highest excited state in some time steps, and the system will be temporarily driven away from the target state (i.e., the ground state of H_p) when its energy has been shifted upwards. In Fig. 10, during the period $\tau \in (0.5, 1.0)$, the order of the ground state and the highest excited state are swapped. Clearly, as shown in the right panel of Fig. 10, the ITE converges to the desired ground state faster in this case.

To avoid the unintended eigenstate re-ordering by the control field, it is crucial to confine the magnitude of β to some proper range. In our test, it is better to set $|\beta|$ to be equal to or less than the magnitude of the energy $\langle \psi(\tau) | H_p | \psi(\tau) \rangle$ which can be obtained from measuring the norm of the matrix problem Hamiltonian. In Fig. 11, we illustrate the effects of choosing different β on the time-evolved energy levels of H_p , which is the Hamiltonian for a two-qubit hydrogen. In this test, we adopt two different approximate bang-bang control strategies $\beta(\tau) = \frac{2S}{1+e^{-\gamma t}} - S$, introduced in Appendix C. These two control strategies share the same γ but $S = 1$ and $S = 10$, respectively. From Fig. 11, it is clear that bigger $|\beta|$ may enlarge energy gaps between eigenstates of H_p but also increases the likelihood of state reordering.

APPENDIX B: EMPIRICAL CONTROL HAMILTONIAN SELECTION

As mentioned in Appendix A, the success of the imaginary-time control (ITC) is to modify this typical evolution path of ITE. The control may drive the time-evolved wave

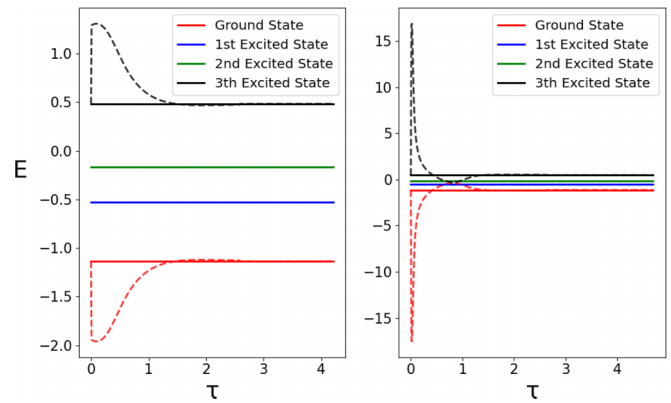


FIG. 11. The result of two-qubit hydrogen with different admissible maximum strength S . It shows that the large admissible maximum strength might decrease the energy gap.

function to temporarily enhance contributions from high-energy eigenstates before converging to the ground state. In other words, the advantage of having controlled dynamics in the imaginary-time domain is to avoid densely spaced energy regions in the Hamiltonian spectrum, which cannot be escaped in the standard ITE. If one can find a H_d that could drive a system towards high-energy states during the ITE, it has the potential to improve the convergence efficiency as prescribed by our proposed method to get ITC.

In this section, we present the strategies of control Hamiltonian selection and discuss how different control Hamiltonian impact the the execution of quantum computing experiments, including empirically control Hamiltonian and simulation results for molecule in Appendix B 1, control Hamiltonian, and control Hamiltonian and simulation results for Sherrington-Kirkpatrick in Appendix B 2, control Hamiltonian and simulation results for a spin model constructed from 3-SAT in Appendix B 3. In summary, with a proper design of control Hamiltonian, we will obtain obvious acceleration for ground state simulation. Thus our proposed imaginary-time control can potentially make a digital quantum simulation for the ground-state preparation much more accessible in the NISQ era.

1. Control Hamiltonian and simulation results for molecule system

Based on the above general strategy for control Hamiltonian selection, here we provide a further empirical method for control Hamiltonian selection, especially for molecule systems. We find that the empirical H_d and its slightly modified versions can greatly speed up the ITC convergence for studied systems with both large and small energy gaps.

For the molecule system, we try the candidate control Hamiltonian H_i containing only Pauli Z (single Z and double Z, and the total number of choices is $C_1^n + C_2^n$ where n is a number of qubits. In studied molecular cases, we find that limiting the Pauli Z to quadratic is enough to obtain greatly speedup.

Intra-molecular bond distance for the typical dissociation curves is considered as an adjustable parameter to generate variant energy gaps for the molecular systems. We choose a

TABLE III. The H_d selection of figures. The function P(S) is the collection of all permutations without repetition of Pauli string S. The I+P(S) means add I before all the Pauli string P(S), for example, II+P(IZ) is equal to {IIIZ, IIZI}. The Full H_d is slightly different from empirical H_d since it has the P(IZ)+I term and the Half H_d is slightly different from the empirical H_d since it lacks the P(ZZ)+I term.

	H_2	H_4	H_6	H_8	LiH	HF
Full H_d	II+P(IZ) P(IZ)+II II+P(ZZ) P(ZZ)+II	III+P(IIIZ) P(IIIZ)+III III+P(IIZZ) P(IIZZ)+III	IIII+P(IIIIZ) P(IIIIZ)+IIII IIII+P(IIIZZ) P(IIIZZ)+IIII	IIIIII+P(IIIIIZ) P(IIIIIZ)+IIIIII IIIIII+P(IIIIZZ) P(IIIIZZ)+IIIIII	IIII+P(IIIIIZ) P(IIIIIZ)+IIIIII IIII+P(IIIIZZ) P(IIIIZZ)+IIIIII	IIIIIIII+P(IZ) P(IIIIIIIZ)+II IIIIIIII+P(ZZ) P(IIIIIIZZ)+II
Half H_d	II+P(IZ) II+P(ZZ)	III+P(IIIZ) III+P(IIZZ)	IIII+P(IIIIZ) IIII+P(IIIZZ)	IIIIII+P(IIIIIZ) IIIIII+P(IIIIZZ)	IIII+P(IIIIIZ) IIII+P(IIIIZZ)	IIIIIIII+P(IZ) IIIIIIII+P(ZZ)
All H_d	P(IIIZ) P(IIZZ)	P(IIIIIZ) P(IIIIZZ)	P(IIIIIIIZ) P(IIIIIIZZ)	P(IIIIIIIIIZ) P(IIIIIIIIIZZ)	P(IIIIIIIIIZ) P(IIIIIIIIZZ)	P(IIIIIIIIIZ) P(IIIIIIIIZZ)
Empirical H_d	II+P(IZ) II+P(ZZ) P(ZZ)+II	III+P(IIIZ) III+P(IIZZ) P(IIZZ)+III	IIII+P(IIIIZ) IIII+P(IIIZZ) P(IIIZZ)+IIII	IIIIII+P(IIIIIZ) IIIIII+P(IIIIZZ) P(IIIIZZ)+IIIIII	IIII+P(IIIIIZ) IIII+P(IIIIZZ) P(IIIIZZ)+IIIIII	IIIIIIII+P(IZ) IIIIIIII+P(ZZ) P(IIIIIIZZ)+II

problem Hamiltonian H_p with a large energy gap as a fast test to help with control Hamiltonian selection. We first run standard ITE on this H_p (which should converge to the ground state easily owing to the large energy gap) and keep a record of the $\beta_i(\tau)$ from the ITE calculation with $|++++\dots++\rangle$ as the initial state. We sum up β_i over time $B_i = \sum_{\tau} \beta_i(\tau)$ for further analysis. From our numerical investigations on molecular systems: H chain, LiH, and HF, we find that those H_i having negative B_i all share the same structure. The structures of Hamiltonian means that, the Pauli strings are divided into two groups that occupy $[0 : (N - 1)]$ and $[N : (M - 1)]$ orbitals respectively, where N is the number of electrons and M is the number of total orbitals. We use these H_i as the control Hamiltonian, which we called *Empirical H_d* . Empirical H_d and its slightly modified versions can ideally great speed up the ITC convergence for studied systems with both large and small energy gaps. Take it for an example, there are 4 electrons ($N = 4$) and 12 total orbitals ($M = 12$), the Pauli strings $P_0P_1P_2P_3P_4P_5P_6P_7P_8P_9P_{10}P_{11}$ will be divided into two groups: $P_0P_1P_2P_3$ IIIIIIII and IIIIP₄P₅P₆P₇P₈P₉P₁₀P₁₁ (for Openfermion notation, the energy of the orbitals from low to high are ordered from left to right). We find that the single Z Pauli strings that Z only exist in $[N : (M - 1)]$ orbitals and the double Z Pauli strings that Zs exist only in $[0 : (N - 1)]$ orbitals or $[N : (M - 1)]$ orbitals have negative B_i (as Table III “Empirical H_d ”), and all other Pauli strings have positive B_i .

Finally, we use the empirical H_d described above for various molecules (H chain, LiH, and HF, see Appendix D) with different energy gaps. In Figs. 12 and 13, we show the ITC results with the control Hamiltonian that has all single Z and double Zs (“control all” in Figs. 12 and 13, “All H_d ” in Table III), the empirical control Hamiltonian mentioned above (“control negative” in Figs. 12 and 13, “Empirical H_d ” in Table III) and the result of the standard ITE (“no control” in Figs. 12 and 13). The results show that the empirical H_d is far better than using all H_i as control Hamiltonian. And empirical H_d can greatly speed up the ITC convergence for studied systems with both large and small energy gaps.

We also test two types of H_d that are slightly different from the empirical H_d mentioned above. The details of those H_d are also listed in Table III. Figure 14 shows the convergence of different types of H_d selections and the speed-up for different

system sizes, where the “Full H_d ” have extra single Z terms compared to “Empirical H_d ” and the “Half H_d ” have less double Z terms compared to “Empirical H_d .” We can see that for “Full H_d ” and “Half H_d ” the acceleration scale approximately exponentially as a function of $1/\Delta E$ for different choices of H_p for the cases we studied on.

2. Control Hamiltonian and simulation results for Sherrington-Kirkpatrick model

Besides the commute basis $\{XX \dots XX, YY \dots YY, ZZ \dots ZZ\}$ we use in the four-qubit cases in the main text. We also construct and compare two types of H_d according to Appendix A 1. One is constructed polynomial H_d from the approximate polynomial basis $p(\tilde{H}_p) = \{\tilde{H}_p^2, \tilde{H}_p^3, \tilde{H}_p^4, \tilde{H}_p^5\}$, where approximate polynomial matrix \tilde{H}_p^k is constructed from

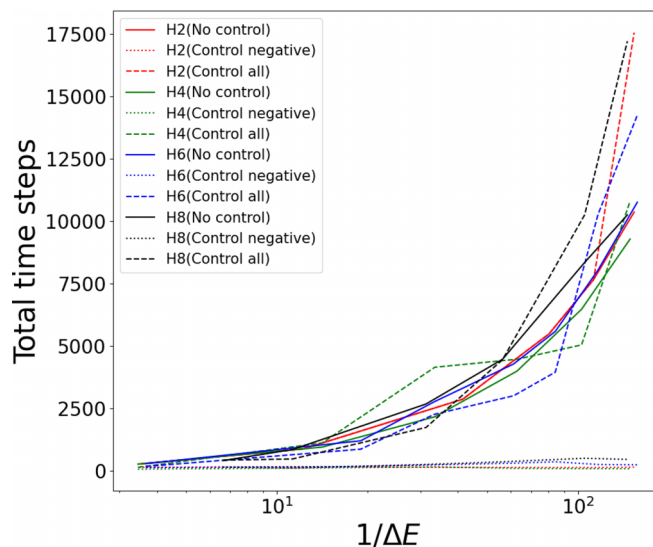


FIG. 12. The result of the control Hamiltonian test of the H chain system, the x axis is a log of $1/\Delta E$, and the y axis is the total time steps for convergence. The result shows that the empirical control Hamiltonian can provide an ITC that gives greatly speed-up with respect to the standard ITE for all cases while H_d that contain all H_i require extra time or no speed-up.

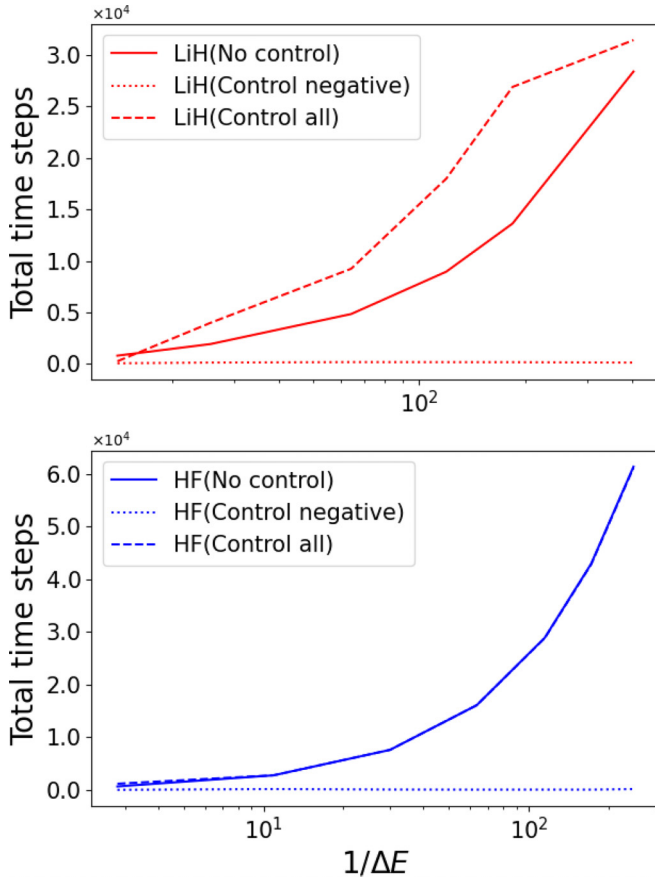


FIG. 13. The result of the control Hamiltonian test of LiH and HF, the x axis is a log of $1/\Delta E$, and the y axis is the total time steps for convergence. The result shows that the empirical control Hamiltonian can provide good control results that have greatly speed-up from ITE for all cases while H_d that contain all H_i require extra time or no speed-up.

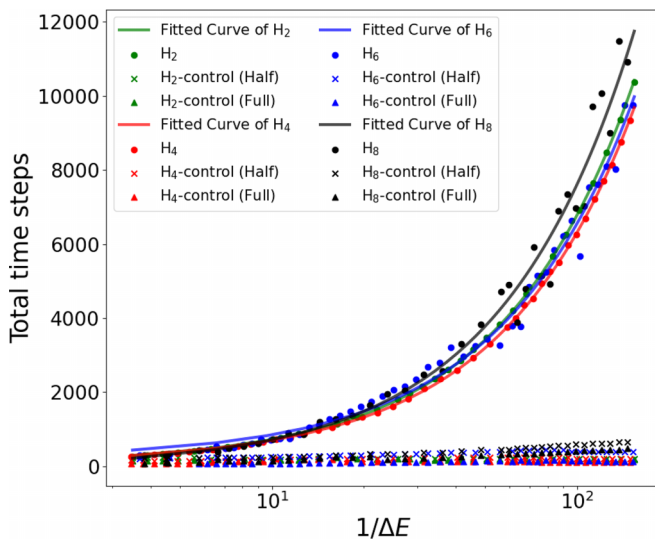


FIG. 14. The result of the H chain size scaling test with different types of H_d . The different dots represent different types of H_d and different colors of lines represent the total time steps.

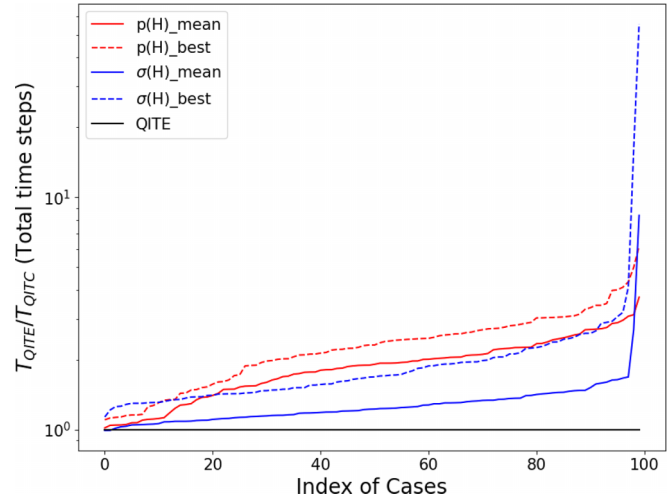


FIG. 15. The result of spin glass (SK model) with different coefficients, the x axis is the case indices sorted by the ratio of total QITE time steps divided by the total QITC time steps, note that sorting does not depend on energy differences. The y axis is the ratio of the total time step. The mean of $p(H)$ and $\sigma(H)$ is the mean of the approximate polynomial H_d and Pauli H_d of ten randomly selected initial states. The best of $p(H)$ and $\sigma(H)$ is the largest speed-up among ten randomly selected initial states using approximate polynomial H_d and Pauli H_d . The single time step $\Delta\tau = 0.03$.

polynomial matrix H_p^k by removing matrix elements that have values less than a fixed constant number. The other Pauli H_d is selected from the 1-local Pauli Z and 4-local Pauli Z *cyclic*(ZIIIII) and *cyclic*(ZZZIIII), where *cyclic* means the set of circular shifts of Pauli strings, for example, *cyclic*(XYZ) = {XYZ, YZX, ZXY}. The control strategy we use here is approximate bang-bang control with the maximum strength of the control field S slowly turning to zero within dozens of time steps to have lower resource requirement, see Appendix C. In Fig. 15, we compared the convergence of ITE and ITC of 100 randomly sampling cases and each case has 10 randomly selected initial states. The result shows that the control can provide a general speed-up and can achieve a hundred times speed-up in some cases. The approximate polynomial H_d can provide a higher average speed-up but weaker corner case speed-up, while Pauli H_d has a lower average speed-up but has a better corner case speed-up.

3. Control Hamiltonian and simulation results for a spin model constructed from 3-SAT

In the main text, we show that ITC can provide obvious speed-up over the ITE for molecular systems. It is also desirable to verify whether such a superior advantage can hold for other scenarios. In this subsection, we compare ITC and ITE for solving a spin model that is closely related to the 3-SAT problems. This is another ground-state preparation task that is sufficiently distinct from the molecular systems considered in the main text.

3-SAT problem is defined by a logical statement involving n boolean variables b_i . The logical statement consists of m clauses C_i in conjunction: $C_1 \wedge C_2 \wedge \dots \wedge C_m$. Each clause is a disjunction of 3 literals, where a literal is a boolean

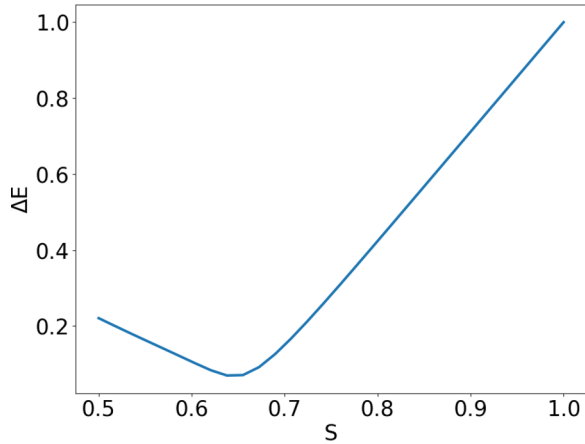


FIG. 16. Annealing 3-SAT instantaneous ΔE , the energy gap between the ground state and first excited state of the time-dependent Hamiltonian $H(s)$.

variable b_i or its negation $-b_i$. For instance, a clause may read $(b_j \vee b_k \vee b_l)$. The task is to first decide whether a given 3-SAT problem is satisfiable; if so, then assign appropriate binary values to satisfy the logical statement. We can map a 3-SAT problem to a Hamiltonian for a set of qubits. Under this mapping, each binary variable b_i is represented as a qubit state. Thus an n -variable 3-SAT problem is mapped into a Hilbert space of dimension $N = 2^n$. Furthermore, each clause of the logical statement is translated to a projector acting on this n -qubit system. Hence, a logical statement with m clauses may be translated to the following Hamiltonian,

$$H_{\text{final}} = \sum_{\alpha=1}^m |b_j^\alpha b_k^\alpha b_l^\alpha j^\alpha\rangle\langle b_j^\alpha b_k^\alpha b_l^\alpha j^\alpha|.$$

A common approach to solve this type of constraint satisfaction problem is to use adiabatic quantum computations(AQC). One first prepares the ground states of an easy-to-solve Hamiltonian H_{init} . Next, one slowly evolves the Hamiltonian such that it adiabatically connects H_{init} and H_{final} . In other words, the adiabatically evolved Hamiltonian reads

$$H(s) = (1 - s)H_{\text{init}} + sH_{\text{final}}, \quad s \in [0, 1],$$

where H_{init} is typically chosen to be a sum of one-qubit Hamiltonians H_i acting on the i th qubit,

$$H_{\text{init}} = \frac{1}{2} \sum_{i=1}^n h_i, \quad h_i = \begin{pmatrix} 1 & -1 \\ -1 & 1 \end{pmatrix}.$$

The energy gap $\Delta E(s)$ between the instantaneous ground state and first-excited state of $H(s)$ will vary with time s as shown in Fig. 16. Based on the well-established theoretical studies, it is also clear that the instantaneous energy gap of interest can get very small along the adiabatic path when the system size is large.

APPENDIX C: THE IMAGINARY-TIME CONTROL STRATEGY

For the imaginary-time control, in this letter, we mainly used two types of control strategy. The first one is the approxi-

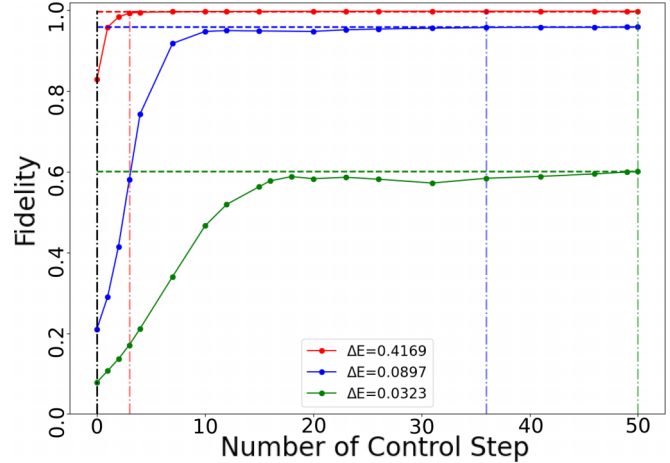


FIG. 17. 50 steps truncation test, the numerical control term truncation test result of eight qubits HF molecule with different energy gap.

mate bang-bang control introduced above that target the larger energy gap problem (type I). The second one is the modified version of the bang-bang strategy that targets the small energy gap problem (type II). We also provide the source codes of all simulations in Ref. [46] where you can find more details on the control strategy and control parameter settings.

1. Imaginary-time control strategy: type I

For the type I control strategy, let us generalize the standard Lyapunov control such that it could work with the imaginary-time evolution. We redefine $T_k \equiv 2\langle \psi | H_p | \psi \rangle \langle \psi | H_d | \psi \rangle - \langle \psi | \{H_p, H_d\} | \psi \rangle$ in this case. The H_d related terms in $T_k(\tau)$ may entail lots of extra measurements if they cannot be obtained by measuring the Pauli terms appearing in $\langle \psi | H_p | \psi \rangle$. To reduce the measurement cost and still maintain a powerful H_d to provide an enhanced convergence, we propose the following strategy. We first decide if the state in the quantum circuit has high overlap with any eigenstate of H_p or H_d by checking the value of T_k , if $T_k < L$ then we do not apply any control pulses, otherwise we use a similar control strategy for the real-time case introduced above.

$$\beta_k(\tau) = \begin{cases} \frac{2S}{1+e^{-\gamma T_k}} - S, & T_k \geq L \\ 0, & \text{else} \end{cases},$$

where L is some predefined threshold value. If the state is close to an eigenstate [i.e., $T_k(\tau) < L$], we should turn off the control field and let the system evolves under H_p in the imaginary-time domain. This truncation can greatly reduce the measurement costs (for the implementation of the corresponding variational algorithm) in the region where the state will linearly converge to the eigenstate. Finally, we test how the truncation [i.e., setting $\beta_k(\tau) = 0$ when $T_k(\tau) < L$] will affect the precision of the converged results given by truncating the control pulse in the middle of the convergence (Fig. 17). For a physical system with a large energy gap between the first-excited state and the ground state, it only requires a few control steps at the beginning then the result of convergence will be very close to the result without truncation. For systems with a small energy gap, the

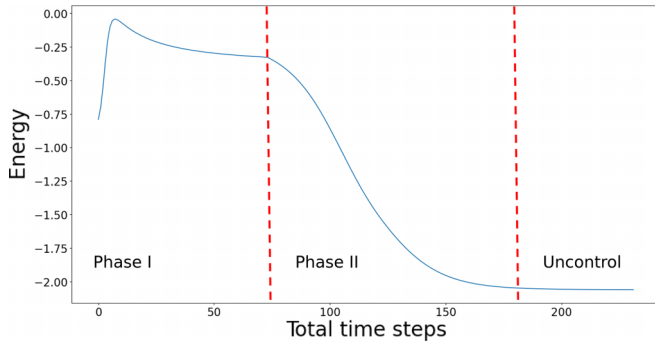


FIG. 18. Two-phase control example, the convergence will pass through three different phases. At phase I, the control will drift the state to a higher energy transition state. In phase II, the control will speed up the convergence to the ground state. In the final phase, the control will be closed to save computing resources.

truncation will significantly affect the precision of the converged results.

2. Imaginary-time control strategy: type II

For the type II control strategy, we use a modified bang-bang control strategy that has two phases. The first phase of control will bypass the slow convergence region and the second phase will speed up the convergence, the demonstration of the phases is demonstrated in Fig. 18. For the small energy gap problem, the type I control might drift the system to the low excited state and weaken the speed-up. To avoid this, we control the state to the transition state that contains high-energy excited state and then to the ground state in two phases. Phase I of the control will lower the contribution of the low-energy states, the energy will go up and reach the equilibrium state consisting of high-energy excited states. Phase two is the traditional bang-bang control which is designed to lower the energy. The switch from phase I to phase II is decided by the energy changes (reach the equilibrium state), and the time-energy plot of the type two control is shown in Fig. 18. In summary, we propose the following control strategy:

$$\beta_k(\tau) = \begin{cases} K_1 \text{sgn}(T_k(\tau)) & \text{(phase 1)} \\ -K_2 \text{sgn}(T_k(\tau)) & \text{(phase 2)} \end{cases}$$

where K_1 and K_2 are the strength of the control field and $\text{sgn}(T_k(\tau))$ is the sign of the $T_k(\tau)$, $\beta_k(\tau)$ will be set to zero if the sign alternating between positive and negative (reach the bound of the H_d), in this paper, we set $K_1 \gg K_2$ to avoid convergence to the excited state.

In conclusion, the advantage of the type I control strategy has weak requirements for the selection of control Hamiltonian, but it may not provide ideally great speed-up of the $1/\Delta E$. The type II control strategy on the other hand can provide greatly speed-up of the $1/\Delta E$ but require stronger control Hamiltonian selection.

APPENDIX D: SYSTEMS HAMILTONIAN

1. Hydrogen

In our simulations, we consider the hydrogen molecule in the minimal STO-3G basis. Each hydrogen atom contributes

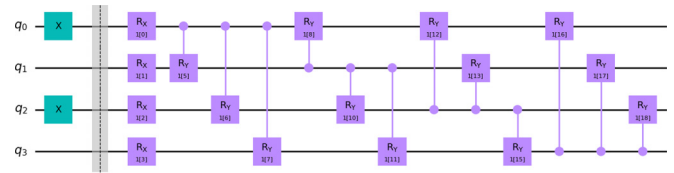


FIG. 19. The variational circuit of four-qubit H_2 system.

a single 1S orbital. As a result of the spin, there are four spin orbitals in total. By using the function of the QISKIT, the qubit Hamiltonian for JW representation can be obtained. This four-qubit Hamiltonian is given by

$$\begin{aligned} H = & h_0 I + h_1 Z_0 + h_2 Z_1 + h_3 Z_2 + h_4 Z_3 + h_5 Z_0 Z_1 \\ & + h_6 Z_0 Z_2 + h_7 Z_0 Z_3 + h_8 Z_1 Z_2 + h_9 Z_1 Z_3 + h_{10} Z_2 Z_3 \\ & + h_{11} Y_0 Y_1 X_2 X_3 + h_{12} Y_0 Y_1 Y_2 Y_3 + h_{13} X_0 X_1 X_2 X_3 \\ & + h_{14} X_0 X_1 Y_2 Y_3 + h_{15} X_0 X_1 Y_2 Y_3. \end{aligned}$$

By using the function of the QISKIT, the two-qubit Hamiltonian of the hydrogen molecule can be obtained from parity representation with Z2 symmetry reduction. This two-qubit Hamiltonian is given by

$$H = h_0 I + h_1 Z_0 + h_2 Z_1 + h_3 Z_1 Z_0 + h_4 X_1 X_0$$

And the circuit (Fig. 19) for Variational-based ansatz [45] simulation used in the main text.

To update the parameters of variational-based ansatz, we calculate the gradient of the circuit by using parameter shift rule [47] to obtain the numerical differential result of the circuit.

2. Hydrogen chain

In our simulations, we consider the hydrogen chain molecule in the minimal STO-3G basis. The hydrogen chain H_n has n electrons and contributes n 1S orbital to the basis.

3. Hydrogen fluoride

In our simulations, we consider the hydrogen fluoride molecule in the minimal STO-3G basis. The fluoride atom has nine electrons, and so contributes a 1S, 2S, $2P_x$, $2P_y$, and $2P_z$ orbital to the basis, while the hydrogen atom contributes a single 1S orbital. For the Appendix B truncation test, by freezing the core two 1S orbitals, we can reduce the system from 12 orbitals with 10 electrons to 8 orbitals with 6 electrons on 2S and 2P orbitals. By using the QISKIT, the qubit Hamiltonian for Jordan-Wigner representation can be obtained. This eight-qubit Hamiltonian is given by 145 different Pauli terms and coefficients.

4. Lithium hydride

In our simulations, we consider the lithium hydride molecule in the minimal STO-3G basis. The lithium atom has three electrons, and so contributes a 1S, 2S, $2P_x$, $2P_y$, and $2P_z$ orbital to the basis, while the hydrogen atom contributes a single 1S orbital.

5. Hamiltonian details for the spin models

The 2D Heisenberg models are constructed with nonperiodic boundary conditions, whose Hamiltonian can be written as

$$H_p = h_i \sum_i Z^i + J_{ij} \sum_{\text{edge}} X^i X^j + Y^i Y^j + Z^i Z^j.$$

The model information in the table presents edge \times edge, for example, 2 \times 2 means 3 \times 3 lattice. The Hamiltonian of

Sherrington-Kirkpatrick model we use can be written as

$$H_p = \sum_{i<j} J_{ij}(X^i X^j + Y^i Y^j + Z^i Z^j)$$

with random generate variables $J_{ij} \in (-0.5, 0.5)$ and using $|++\dots\rangle$ as the initial state.

-
- [1] T. Monz *et al.*, Realization of a scalable Shor algorithm, *Science* **351**, 1068 (2016).
- [2] M. Schaden, Quantum finance, *Physica A* **316**, 511 (2002).
- [3] J. Biamonte *et al.*, Quantum machine learning, *Nature (London)* **549**, 195 (2017).
- [4] S. McArdle *et al.*, Quantum computational chemistry, *Rev. Mod. Phys.* **92**, 015003 (2020).
- [5] B. Bauer *et al.*, Quantum algorithms for quantum chemistry and quantum materials science, *Chem. Rev.* **120**, 12685 (2020).
- [6] A. Peruzzo *et al.*, A variational eigenvalue solver on a photonic quantum processor, *Nat. Commun.* **5**, 4213 (2014).
- [7] H. Grimsley *et al.*, An adaptive variational algorithm for exact molecular simulations on a quantum computer, *Nat. Commun.* **10**, 3007 (2019).
- [8] O. Higgott, D. Wang, and S. Brierley, Variational quantum computation of excited states, *Quantum* **3**, 156 (2019).
- [9] M. Cerezo *et al.*, Variational quantum algorithms, *Nat. Rev. Phys.* **3**, 625 (2021).
- [10] A. Kitaev, Quantum measurements and the Abelian stabilizer problem, [arXiv:quant-ph/9511026v1](https://arxiv.org/abs/quant-ph/9511026).
- [11] M. Dobřiček *et al.*, Arbitrary accuracy iterative quantum phase estimation algorithm using a single ancillary qubit: A two-qubit benchmark, *Phys. Rev. A* **76**, 030306(R) (2007).
- [12] N. Wiebe and C. Granade, Efficient Bayesian Phase Estimation, *Phys. Rev. Lett.* **117**, 010503 (2016).
- [13] T. E. O'Brien, T. Brian, and M. T. Barbara, Quantum phase estimation of multiple eigenvalues for small-scale (noisy) experiments, *New J. Phys.* **21**, 023022 (2019).
- [14] N. Gomes *et al.*, Efficient step-merged quantum imaginary time evolution algorithm for quantum chemistry, *J. Chem. Theory Comput.* **16**, 6256 (2020).
- [15] M. Motta *et al.*, Determining eigenstates and thermal states on a quantum computer using quantum imaginary time evolution, *Nat. Phys.* **16**, 205 (2020).
- [16] S. McArdle *et al.*, Variational ansatz-based quantum simulation of imaginary time evolution, *npj Quantum Inf.* **5**, 75 (2019).
- [17] M. Beach *et al.*, Making trotters sprint: A variational imaginary time ansatz for quantum many-body systems, *Phys. Rev. B* **100**, 094434 (2019).
- [18] X. Yuan *et al.*, Theory of variational quantum simulation, *Quantum* **3**, 191 (2019).
- [19] K. Seki and S. Yunoki, Quantum power method by a superposition of time-evolved states, *PRX Quantum* **2**, 010333 (2021).
- [20] O. Kyriienko, Quantum inverse iteration algorithm for programmable quantum simulators, *npj Quantum Inf.* **6**, 7 (2020).
- [21] J. R. McClean *et al.*, Barren plateaus in quantum neural network training landscapes, *Nat. Commun.* **9**, 4812 (2018).
- [22] E. Grant *et al.*, An initialization strategy for addressing barren plateaus in parametrized quantum circuits, *Quantum* **3**, 214 (2019).
- [23] M. Cerezo *et al.*, Cost function dependent barren plateaus in shallow parametrized quantum circuits, *Nat. Commun.* **12**, 1791 (2021).
- [24] S. Wang *et al.*, Noise-induced barren plateaus in variational quantum algorithms, *Nat. Commun.* **12**, 6961 (2021).
- [25] Z. Holmes *et al.*, Barren Plateaus Preclude Learning Scramblers, *Phys. Rev. Lett.* **126**, 190501 (2021).
- [26] S. Kuang and C. Shuang, Lyapunov control methods of closed quantum systems, *Automatica* **44**, 98 (2008).
- [27] X. Wang and G. S. Sophie, Analysis of Lyapunov method for control of quantum states, *IEEE Trans. Autom. Control* **55**, 2259 (2010).
- [28] D. Dong and I. R. Petersen, Quantum control theory and applications: a survey, *IET Control Theory Applic.* **4**, 2651 (2010).
- [29] S. Cong and M. Fangfang, A survey of quantum Lyapunov control methods, *The Scient. World J.* **2013**, 967529 (2013).
- [30] B. A. Magann *et al.*, Feedback-Based Quantum Optimization, *Phys. Rev. Lett.* **129**, 250502 (2022).
- [31] A. B. Magann *et al.*, Digital quantum simulation of molecular dynamics and control, *Phys. Rev. Res.* **3**, 023165 (2021).
- [32] V. Ramakrishna *et al.*, Controllability of molecular systems, *Phys. Rev. A* **51**, 960 (1995).
- [33] A. del Campo, M. Rams, and W. Zurek, Assisted Finite-Rate Adiabatic Passage Across a Quantum Critical Point: Exact Solution for the Quantum Ising Model, *Phys. Rev. Lett.* **109**, 115703 (2012).
- [34] Y. Chen *et al.*, Optimizing quantum annealing schedules: From Monte Carlo tree search to quantumzero, [arXiv:2004.02836](https://arxiv.org/abs/2004.02836).
- [35] D. D'Alessandro, *Introduction to Quantum Control and Dynamics* (Chapman and Hall/CRC Press, 2021).
- [36] S. Grivopoulos and B. Bamieh, in *Proceedings of the 42nd IEEE International Conference on Decision and Control* (IEEE, New York, 2003), Vol. 1, pp. 434–438.
- [37] S. Kuang, D. Dong, and I. R. Petersen, Approximate bang-bang Lyapunov control for closed quantum systems, in *Proceedings of the 2014 4th Australian Control Conference (AUCC)* (IEEE, New York, 2014), pp. 124–129.
- [38] S. G. Schirmer, H. Fu, and A. I. Solomon, Complete controllability of quantum systems, *Phys. Rev. A* **63**, 063410 (2001).
- [39] F. Albertini and D. D'Alessandro, Notions of controllability for bilinear multilevel quantum systems, *IEEE Trans. Autom. Control* **48**, 1399 (2003).
- [40] G. M. Huang, T. Tarn, and J. Clark, On the controllability of quantum-mechanical system, *J. Math. Phys.* **24**, 2608 (1983).

- [41] C. Zhang, D. Dong, and Z. Chen, Control of non-controllable quantum systems: A quantum control algorithm based on Grover iteration, *J. Opt. B: Quantum Semiclass. Opt.* **7**, S313 (2005).
- [42] A. D. McLachlan, A variational solution of the time-dependent Schrodinger equation, *Mol. Phys.* **8**, 39 (1964).
- [43] J. Broeckhove *et al.*, On the equivalence of time-dependent variational principles, *Chem. Phys. Lett.* **149**, 547 (1988).
- [44] S. Zhang *et al.*, TensorCircuit: A quantum software framework for the NISQ Era, *Quantum* **7**, 912 (2023).
- [45] S. Sim, J. D. Peter, and A. Aspuru-Guzik, Expressibility and entangling capability of parameterized quantum circuits for hybrid quantum-classical algorithms *Adv. Quantum Tech.* **2**, 1900070 (2019).
- [46] <https://github.com/Kesson-C/QITC>.
- [47] M. Schuld *et al.*, Evaluating analytic gradients on quantum hardware, *Phys. Rev. A* **99**, 032331 (2019).